Proceedings of the ASME 2023 42nd International Conference on Ocean, Offshore and Arctic Engineering
OMAE2023
June 11-16, 2023, Melbourne, Australia

OMAE2023-100743

HOW LOADS INTERACT? A NUMERICAL INVESTIGATION OF ALUMINUM STIFFENED PANELS UNDER BI-AXIAL AND LATERAL LOADS

Xintong Wang
Centre of Autonomous Marine Operation and Systems,
Department of Marine Technology,
Norwegian University of Science and Technology,
Trondheim, Norway

Jørgen Amdahl
Centre of Autonomous Marine Operation and Systems,
Department of Marine Technology,
Norwegian University of Science and Technology,
Trondheim, Norway

ABSTRACT

Due to low weight, aluminum alloys are commonly used to build ferries, working boats and high-speed ships. The hull of such vessels can be designed as catamaran and trimaran for favorable hydrodynamical behavior and operational purposes. Non-monohull structures are in certain areas more exposed to combined loads, such as the cross-deck subjected to the longitudinal and transverse hull bending, and water slamming. In these cases, the existing design rules predict the ultimate strength with simplified interactions between bi-axial and lateral loads. A further complicating effect is the reduced material strength and residual stresses in the heat affected zones (HAZ). Thus, it is still necessary to investigate the ultimate strength of aluminum stiffened panels subjected to combined loads and get a better understanding of the interaction mechanics, which again may lead to improved design rules.

Based on a previously developed numerical model, the structure response of an aluminum multi-span panel subjected to combined longitudinal, transverse, and lateral loads is simulated with the nonlinear finite element method. The welding effects are considered, including both geometrical and mechanical imperfections. By changing the combined load values, the interactions between bi-axial loads are examined. The influences of lateral pressure level on the structure response are also investigated. The failure process, ultimate strength, and stress components between different cases are compared.

Keywords: Aluminum; Stiffener panel; Bi-axial load; Lateral pressure; Ultimate strength; Welding effects

1. INTRODUCTION

Aluminum alloys are typically employed in building ferries, working boats and high-speed vessels with higher strength-to-weight ratio compared to steels. For favorable hydrodynamic behavior and operational purposes, the hull of such vessels can be designed as catamaran and trimaran. Nonetheless, such non-monohull structures in certain areas are more exposed to combined loads, such as the cross-deck subjected to longitudinal and transverse bending, and water slamming. The interactions between the loads influence the structure failure mode noticeably, but the governing mechanical behavior are difficult to be determined in detail considering varying loading paths from different combinations. In the design stage, only simplified interactions between bi-axial, shear and lateral loads are normally assumed in closed form methods to evaluate the structure strength of stiffen panels. In addition, the material softening and residual stresses in the heat affected zones (HAZ) are also influential and complicated for aluminum structures.

To understand the compressive ultimate strength of the aluminum ship structures together with welding effects, extensive research has been conducted. The progresses, challenges and future research needs have been well reviewed in the work by Liu et. al. [1], and Hosseinabadi and Khedmati [2]. As for the scenarios where the combined loads are considered, the related research work is still limited. There is no experiment of aluminum stiffened panels subjected to combined loads, partly due to difficulties of designing loading methods/instruments. The researchers mainly use finite element methods to investigate the structure behavior with bi-axial loads, shear and lateral pressure [3-9]. It has been addressed that the transverse and lateral load change the buckling mode as changing the boundary conditions when the loads are beyond certain levels. Based on the obtained numerical results, some empirical formulations for ultimate strength prediction have been developed [4, 7]. In the developed analytical or semi-analytical methods, the orthotropic plate theory has been mainly used as a foundation together with numerical integrations to predict the structure behavior [10-12]. One of successful applications has been concluded as DNV PULS [13-16].

In the design stage, the structure strength is normally fast evaluated by the closed form methods from the classification rules. Some of them were originally developed for steel structures and the adoption to the aluminum structures needs to be checked carefully. Even for the steel structures, the response under the combined loads is not fully understood. The recent change of the IACS Common Structural Rules for Bulk Carriers and Oil Tankers, from the beam-based formulae to the orthotropic-plate-based formulae, to further improve the accuracy under combined stresses [17], could somehow reflect such a knowledge shortage. Thus, the investigation of the aluminum structure behavior under the combined loads, together with the welding effects, is still necessary.

In this work, an aluminum multi-span panel subject to combined longitudinal compression, transverse compression, and lateral pressure are simulated with the nonlinear finite element method. The welding effects are also modelled, including both geometrical and mechanical imperfections, based on a previously verified numerical model. By changing the load combinations, the failure modes, failure process, and ultimate strength are investigated. The numerical predictions are compared with the design rules and are further discussed. The interaction between the bi-axial loads and lateral pressure is examined through the stress components at the ultimate strength point.

2. NUMERICAL MODELLING

2.1 Geometries and welding effects

The multi-span stiffened panel in the simulations included two complete and two half spans. The cross-section of the plate, stiffeners and frames were determined based on an operating aluminum catamaran and marine standard extruded items by Hydro [18]. The stiffened panel consisted of a L-profile with associated plate flange and was welded to the adjacent stiffeners at edges (mid between stiffeners). The width of the HAZ was 40 mm. The detailed geometry is shown in Figure 1. Local buckling of stiffener web and frames was avoided by satisfying the requirements from DNV-RP-C201 and checked by test runs.

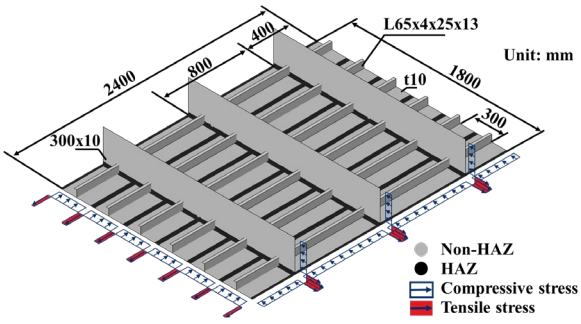

FIGURE 1: MODEL GEOMETRIES AND MECHANICAL IMPERFECTIONS

The welding effects in the model included the mechanical and geometrical imperfections. The mechanical imperfections were assigned based on the HAZ, within which softened material properties and tensile residual stresses were applied, while outside which base material properties and compressive residual stresses were adopted as shown in Figure 1. The AA6082-T6 aluminum alloys were modelled through the Ramberg-Osgood relationships in the simulations as:

$$E\varepsilon = \sigma + \alpha\left(\frac{|\sigma|}{\sigma^0}\right)^{n-1}\sigma \tag{1}$$

where E is the Young's modulus, ε is the strain, σ is the stress, α is the 'yield' offset, σ^0 is the yield stress, and n is the hardening exponent for the plastic term. The material parameters were calibrated to experiments by Aalberg et. al [19]. The base material of the plate, of the stiffeners and frames, and softened material in the HAZ used different material properties as shown in Table 1 and Figure 2.

Table 1: Material parameters

	E [MPa]	σ^0[MPa]	α[-]	n[-]
Plate		309	0.405	179
Stiffeners/Frames	62612	302	0.415	58.8
HAZ		185.41	0.675	16.3

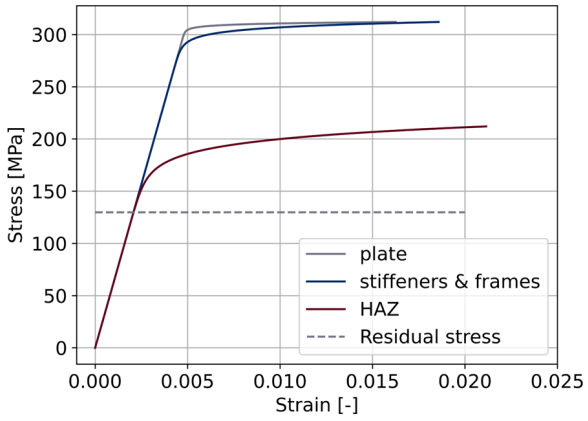

FIGURE 2: STRESS-STRAIN CURVES

The geometrical imperfections were assigned by moving nodes individually. Three half-sinusoidal waves longitudinally and one half-sinusoidal wave transversely were assumed for the plate deflection between stiffeners and frames, denoted as w_{pl}. One half-sinusoidal wave was assumed for the stiffened plate deflection between frames and stiffener sideway deflection, denoted as w_{pg} and w_{st} as illustrated in Figure 3 with hidden frames. The imperfection amplitudes were determined from DNV-OS-C401 Fabrication and Testing of Offshore Structures [20] as:

$$w_{pl} = 0.005s \tag{2}$$

$$w_{pg} = 0.0015\mathrm{L} \tag{3}$$

$$w_{st} = 0.002\mathrm{L} \qquad (4)$$

, where L and s are the frame and stiffener spacing, respectively.

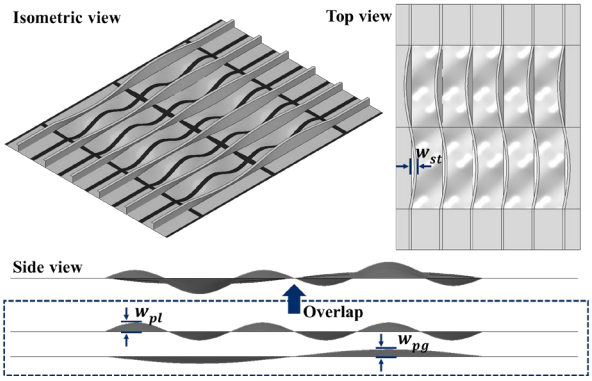

FIGURE 3: GEOMETRICAL IMPERFECTIONS OF THE MODEL (MAGNIFIED 50 TIMES)

The imperfection shapes were assumed continuous across the frame to ensure the critical cases for buckling. It is claimed that the widely accepted imperfection field and the value of the aluminum stiffened panel are still lacking, and they influence the structure behavior substantially. It is noticed that the local plate imperfection in this case is larger than the commonly used formulae, 0.0015L. Such an assumption ensures the critical cases for the combined load effect investigation.

2.2 Loads and boundary conditions

The longitudinal direction was set as the primary loading direction as shown in Figure 4. The transverse stress and the lateral pressure were applied first with the chosen value. Subsequently, a displacement-controlled compression with a velocity of 1 mm/s was applied until the structure failed. The existence of inertia forces was found influential in the choice of failure path between several closely spaced solutions [21]. The loading velocity in this work was chosen based on test runs.

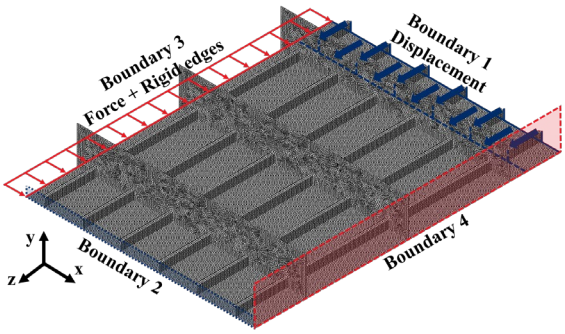

FIGURE 4: APPLIED LOADS IN THE SIMULATIONS

The transverse stress was applied along the plate edges by the 'Shell edge load'. The 'Kinematic coupling constraints' were imposed to keep such boundaries straight. The lateral pressure was assigned on the outer surface of the panel plate. The stiffened panel boundaries are assumed supported by the neighboring strong frames and thus rotational fixed. The detailed boundary conditions are given in the Table 2. The 'U' and 'R' denotes the displacement and rotation, respectively.

Table 2: Boundary conditions

Boundary	Ux	Uy	Uz	Rx	Ry	Rz
1	Free	Fixed	Disp.	Fixed	Fixed	Fixed
2	Free	Fixed	Fixed	Fixed	Fixed	Fixed
3	Free	Fixed	Free	Fixed	Fixed	Fixed
1	Fixed	Fixed	Free	Fixed	Fixed	Fixed

2.3 Mesh and result contrast

The S4R element was used to mesh the structure. It is a linear quadrilateral element with reduced integration. Some S3, linear triangular, elements also existed around the plate-stiffener-frame interactions. The 'Dynamic, Implicit' solver was employed with the 'Quasi-static' application. The solver includes the inertia effects, which is beneficial to overcome instabilities. It was successfully used to simulate aluminum panel buckling [21, 22].

The mesh size sensitivity was analyzed in two cases, with and without the combined loads, as shown in Figure 5. A mesh size of 10 mm was selected considering a balance between the result accuracy and computational time. It was noticed that the structure would vibrate after the ultimate strength points, especially when the mesh size is small. It is attributed to the use of explicit dynamic solver with inertia forces, and a small density of aluminum alloys. The behavior after the ultimate strength point was not focused on in this work; the simulations would be stopped automatically during the vibration by a set-up maximum step number. The numerical model in in this work used the same mesh size and HAZ model as those in the previous work by authors, in which the most predicted ultimate strength differed less than 10% compared to that from reference experiments [21].

The obtained ultimate strength from the test run without the combined loads was compared with the structure strength predictions from the closed form methods in the design rules, as shown in Figure 5. The compared rules included DNV-RP-C201, DNV-CG-0128 (new and old) [23, 24], Eurocode9 [25] and DNV-RU-HSLC [26]. The predicted ultimate strength of the numerical simulation was 6%, 8%, 12%, 23% and 34% larger than the design resistance from the rules. It is noted that the first two rules were developed for steel structures, while the latter two for aluminum structures. The rules predicted a stiffener induced failure or stiffener side failure as the most critical failure mode, which was same as the upward deformed panel in the simulation. Considering the buckling mode consistency and accepted ultimate strength difference with the most design rules, it was concluded that the numerical model could reflect the critical cases in the reality and could be used for the investigation in this work.

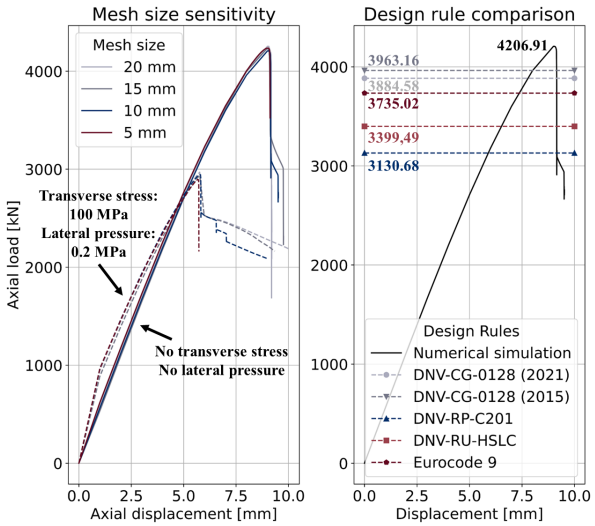

FIGURE 5: NUMERICAL SIMULATION VERIFICATIONS

The most conservative prediction was obtained with the DNV-RP-C201 formulation. This rule was reported to predict conservative resistance (50% smaller), compared to numerical simulations for slender steel structures [27]. Noticing that aluminum panels have the slenderness magnified by $\sqrt{3}$ compared to steel structures with the same geometry due to a different Young's modulus. The plate slenderness in this case is approximate two. In the DNV-RP-C201, it results in a small effective width of the attached plate, thus a conservative design resistance.

In the Eurocode 9, a thickness reduction based on the yield stress of the plate and stiffener was applied, to take into account local buckling. If the yield stress of softened material is used, the difference would be 0.09% instead of 12%. It means that in the rule a lower yield stress in the HAZ decreases the possibility of local buckling, increases the total resistance, also better coincides with the numerical simulation.

3. RESULTS AND DISCUSSIONS

In the numerical simulation cases, the applied transverse stress varied from 0 to 100 MPa in steps of 25 MPa, providing that the ultimate strength for transverse compression is approximate 136 MPa**.** The applied lateral pressure varied from 0 to 0.2 MPa in steps of 0.05 MPa. The first yield pressure of the stiffener with attached plate is approximate 0.4 MPa. The results are extracted and discussed in this section.

3.1 Failure processes

The longitudinal buckling stress of the plate between stiffeners is around 70 MPa. The elastic plate buckling happens after the stress exceeds the critical value. The stiffeners are subjected to bending moment due to the lost capacity of the plate. This can be confirmed by the non-uniform membrane stress distribution within the plate before any materials yield.

Then, the ultimate strength of the panel is obtained when the stiffener fails under the bending. After the plate buckles, the material of the stiffener yields first at the top at the stiffener-frame interaction. Then the yield area extends to the bottom, and further develops along plate-frame connections. It makes the stiffeners with the attached plate deform as simply supported and promotes the stiffener buckling. It is noticed that the material at the plate-stiffener connection in the mid-span may yield right after or simultaneously with the buckling, depending on the combined load level. Further loading after the buckling promotes the total yielding of the stiffener, resulting in large structure deformations. The general failure process is shown by the yield area development in Figure 6.

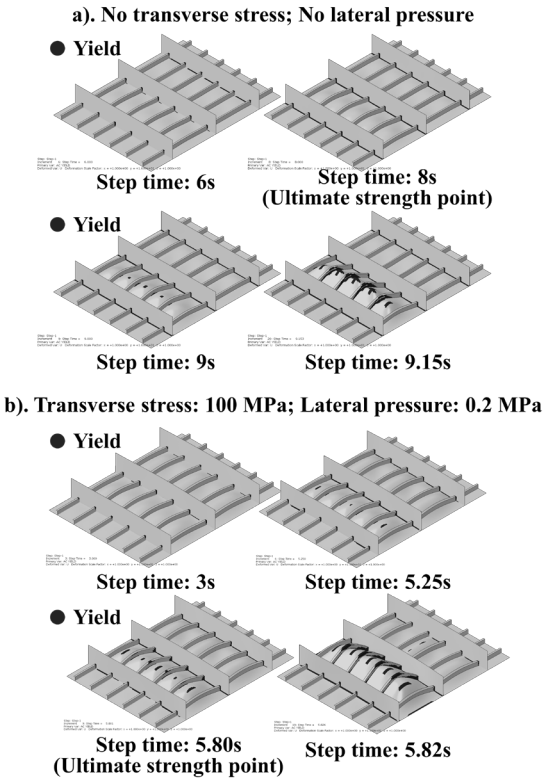

FIGURE 6: YIELD AREA DEVELOPMENT OF TYPICAL CASES (VERTICAL DEFLECTION X10)

It is noticed that the failure processes are slightly different at the beginning. The vertical translation at the first timestep is displayed in Figure 7 where the frames are hidden. The stiffened panel basically deforms with the initial imperfection shape. For the cases without lateral pressure, local plate imperfection dominates. The assignment of the lateral pressure changes the response to the global plate imperfection, but the introduced transverse stress could retard the change. Although the deflection shape varies at the beginning, the global plate imperfection dominates with the increasing longitudinal compression, thus resulting in the similar failure mode for all cases.

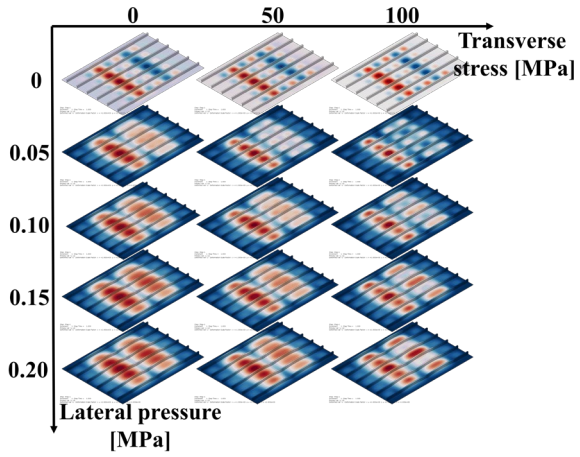

FIGURE 7: VERTICAL TRANSLATIONS AT FIRST TIME STEP (VERTICAL DEFLECTION X10)

3.2 Load end-shortening curves

The load end-shortening in longitudinal direction is plotted in Figure 8. The peak value is regarded as the ultimate strength in such case. Both with the increasing transverse stress and lateral pressure, the ultimate strength decreases. When the stiffened panel is subject to transverse force, the load end-shortening curves show a clear yield point. An increasing transverse stress results in a higher yielding point and stronger linear section because of the biaxial stress state, as shown in the zoomed view. The lateral pressure changes behavior after the yield point mainly if the transverse force applies. Otherwise, the whole curve is changed from the beginning.

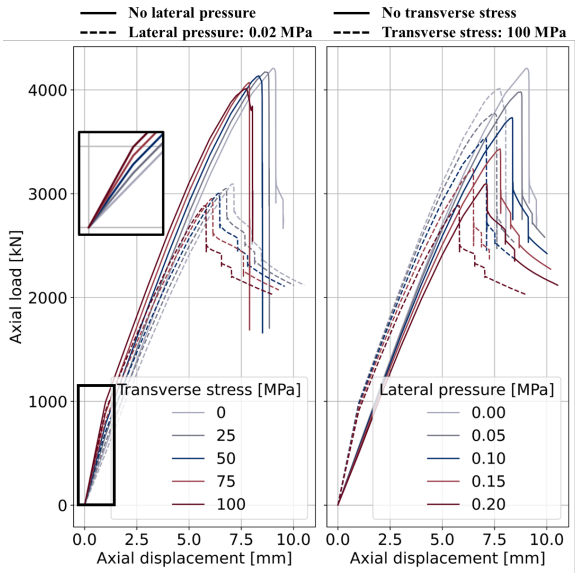

FIGURE 8: LOAD END-SHORTENING CURVES

The ultimate strength for combined loading from the simulation cases and resistance predicted using DNV-CG-0128 code from 2015- and 2021-version are plotted in Figure 9. The design resistance shows obvious difference between codes when the combined loads are assigned. The variation increases with larger load values.

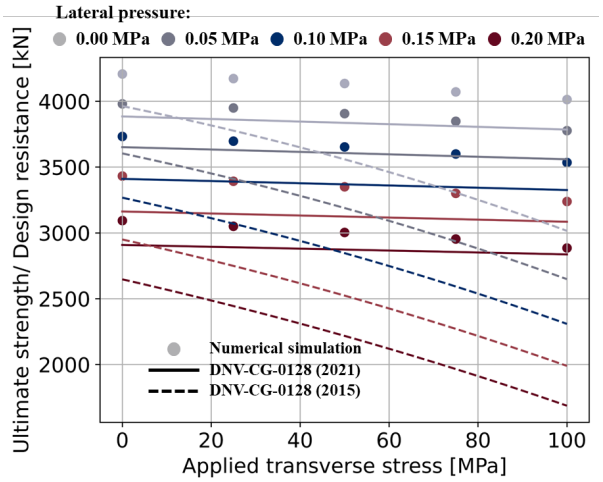

FIGURE 9: COMPARISON BETWEEN PREDICTED ULTIMATE STRENGTH AND DESIGN RESISTANCE

The resistance from the 2015-verision shows a significant reduction due to transverse stress while that from the 2021-version is less influenced by transverse stress and agree better with the numerical simulations. In the 2021-version, the bending moment due to the lateral deformation of the stiffener is modified. The stress is scaled from the global elastic buckling capacity of the stiffened panel instead of the equivalent lateral load of the attached plate at mid span. In the latter case, the stiffener is neglected when evaluating the load, which is too conservative for combined load cases.

A less conservation from the 2021-verision is noticed with a larger lateral pressure. The reason is the boundary condition transition in the numerical simulations. The stiffener ends change from simply-supported-like to clamped-like with an increased lateral pressure, resulting in a lower ultimate strength. It reveals that the combined loads may influence boundary conditions and the assumption in the closed method should be chosen carefully.

3.3 Membrane and bending stresses

At the failed plate midspan, the longitudinal stress values are extracted along the cross-section at the ultimate strength point. The membrane σ_{mem} and bending σ_{ben} stress in the plate can be calculated from the finite element results as:

$$\sigma_{mem} = (\sigma_{top} + \sigma_{bottom})/2 \quad (5)$$

$$\sigma_{ben} = (\sigma_{top} - \sigma_{bottom})/t \quad (6)$$

, where the σ_{top} is the stress value at the top integration point and the σ_{bottom} is the stress value at the bottom integration point. The membrane stress and bending stress are plotted in Figure 10.

The stiffener positions are marked with the dashed lines. A generally symmetric stress distribution is observed for the whole panel so only half is shown for simplicity. In between the stiffeners, the plate is mainly under compression. At the plate-stiffener connections, tensile membrane stress and bending stress exist due to the support from the stiffeners. It shows that the stiffeners in the studies cases are subjected to a strong bending moment.

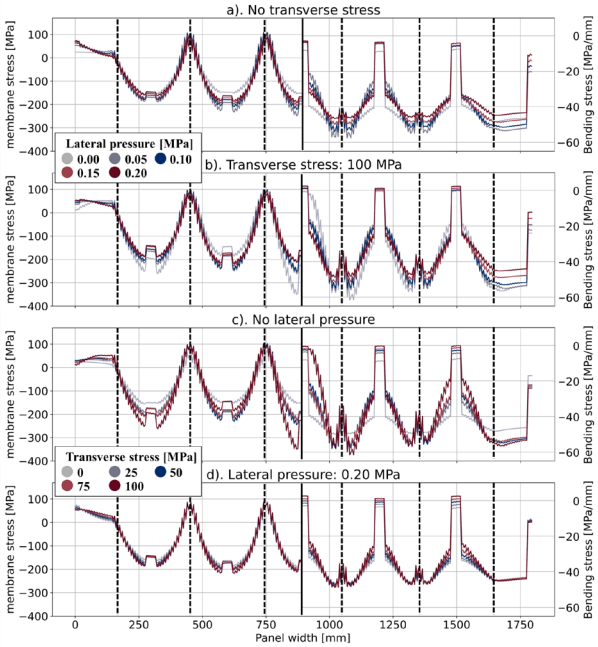

FIGURE 10: MEMBRANE STRESS (LEFT) AND BENDING STRESS (RIGHT) IN THE LONGITUDINAL DIRECTION AT THE PLATE MIDSPAN

The stress distribution changes little with different load levels because of the similar failure mode. The lateral pressure mainly amplifies the magnitude. The transverse stress intensifies the uneven global distribution. The plate area at the middle width is focused with limited influences from the boundaries. When there is no transverse stress, a lateral pressure of 0.05 MPa increases the membrane stress and decreases the bending stress. A further increment has opposite influences, but minor. The influence from the lateral pressure is also obvious when there is a transverse stress up to 100 MPa. Without the lateral pressure, the transverse force reduces the stresses within in the plate, while it influences little when large lateral pressure dominates.

The HAZ model influences the stress distribution obviously. Both the membrane and bending stress show a constant and reduced part within the HAZ. The bending stress is more vulnerable, resulting in an area almost without values. The assumed tensile residual stress is believed to cause it.

4. CONCLUSION

Through the nonlinear finite element analysis of the aluminum stiffened panels subjected to bi-axial loads and lateral pressure, the interactions between combined loads are investigated with focuses on the failure processes, load end-shortening curves and stress components at the ultimate strength point. Main conclusions from the work are summarized as:

- The applied combined load doesn't change the failure mode in this study, but slightly influence the failure process at the beginning. The introduction of the lateral pressure changes the dominated deflection mode from the local plate imperfection to the global plate imperfection.
- Compared to the numerical simulations, the 2021-version DNV-CG-0128 gives better predictions than the 2015-version when the bi-axial and lateral load are assigned. The modified method to calculate the stiffener bending moment due to the lateral deformation is more accurate.
- Most areas of the plate are under compression in this study, but the tensile state exists at the plate-stiffener connections. The stiffener is subjected to a bending stress mainly. An increased lateral pressure aggravates the compression and mitigates the bending, while an increased transverse force only increases the membrane stress.
- The HAZ model influences the stress state obviously. The assumed tensile residual stresses of the butt welding in this work reduces the compressive stress and almost eliminates the bending stress of the plate within the HAZ.

ACKNOWLEDGEMENTS

The authors gratefully acknowledge the support from the Research Council of Norway under the Knowledge-Building Project for Industry Robot Welding of Aluminum Ship Hulls [grant number: KPN295138]. Part of this work is also supported by the Centre for Autonomous Marine Operations and Systems (AMOS) [project number: 223254]. We are grateful to the support from high performance computation resources of the Norwegian national e-infrastructures, Project NN9585K - Accidental actions on strait crossings and offshore platforms.

REFERENCES

[1] Liu, B., Doan, V. T., Garbatov, Y., Wu, W., and Guedes Soares, C., 2020, "Study on Ultimate Compressive Strength of Aluminium-Alloy Plates and Stiffened Panels," Journal of Marine Science and Application.

[2] Hosseinabadi, O. F., and Khedmati, M. R., 2021, "A review on ultimate strength of aluminium structural elements and systems for marine applications," Ocean Engineering, 232, p. 109153.

[3] Khedmati, M. R., Zareei, M. R., and Rigo, P., 2009, "Sensitivity analysis on the elastic buckling and ultimate strength of continuous stiffened aluminium plates under combined in-plane compression and lateral pressure," Thin-Walled Structures, 47(11), pp. 1232-1245.

[4] Khedmati, M. R., Zareei, M. R., and Rigo, P., 2010, "Empirical formulations for estimation of ultimate strength of continuous stiffened aluminium plates under combined in-plane compression and lateral pressure," Thin-Walled Structures, 48(3), pp. 274-289.

[5] Khedmati, M. R., Bayatfar, A., and Rigo, P., 2010, "Post-buckling behaviour and strength of multi-stiffened aluminium panels under combined axial compression and lateral pressure," Marine Structures, 23(1), pp. 39-66.
[6] Khedmati, M. R., Pedram, M., and Rigo, P., 2014, "The effects of geometrical imperfections on the ultimate strength of aluminium stiffened plates subject to combined uniaxial compression and lateral pressure," Ships and Offshore Structures, 9(1), pp. 88-109.
[7] Khedmati, M. R., Memarian, H. R., Fadavie, M., and Zareei, M. R., 2016, "Empirical formulations for estimation of ultimate strength of continuous aluminium stiffened plates under combined transverse compression and lateral pressure," Ships and Offshore Structures, 11(3), pp. 258-277.
[8] Syrigou, M., Benson, S., and Dow, R., 2015, "Strength of aluminium alloy ship plating under combined shear and compression/tension," Analysis and Design of Marine Structures V, CRC Press, pp. 487-496.
[9] Syrigou, M. S., and Dow, R. S., 2018, "Strength of steel and aluminium alloy ship plating under combined shear and compression/tension," Engineering Structures, 166, pp. 128-141.
[10] Paik, J. K., Thayamballi, A. K., and Ju Kim, B., 2001, "Large deflection orthotropic plate approach to develop ultimate strength formulations for stiffened panels under combined biaxial compression/tension and lateral pressure," Thin-Walled Structures, 39(3), pp. 215-246.
[11] Paik, J. K., and Lee, M. S., 2005, "A semi-analytical method for the elastic–plastic large deflection analysis of stiffened panels under combined biaxial compression/tension, biaxial in-plane bending, edge shear, and lateral pressure loads," Thin-Walled Structures, 43(3), pp. 375-410.
[12] Benson, S., Downes, J., and Dow, R. S., 2013, "Compartment level progressive collapse analysis of lightweight ship structures," Marine Structures, 31, pp. 44-62.
[13] Byklum, E., and Amdahl, J., 2002, "A simplified method for elastic large deflection analysis of plates and stiffened panels due to local buckling," Thin-Walled Structures, 40(11), pp. 925-953.
[14] Byklum, E., 2002, Ultimate strength analysis of stiffened steel and aluminium panels using semi-analytical methods, Fakultet for ingeniørvitenskap og teknologi.
[15] Byklum, E., Steen, E., and Amdahl, J., 2004, "A semi-analytical model for global buckling and postbuckling analysis of stiffened panels," Thin-Walled Structures, 42(5), pp. 701-717.
[16] PULS, D., 2006, "User's manual (version 2.05)," Technical Report.
[17] IACS, 2020, "Common Structural Rules for Bulk Carriers and Oil Tankers - Technical Background for Rule Change Notice 1 to 01 JAN 2020 version."
[18] Hydro, 2019, "Technical datasheet - Extruded products Alloy EN AW-6082 [AlSi1MgMn]."
[19] Aalberg, A., Langseth, M., and Larsen, P. K., 2001, "Stiffened aluminium panels subjected to axial compression," Thin-Walled Structures, 39(10), pp. 861-885.
[20] Veritas, D. N., 2014, "DNV-OS-C401 Fabrication and Testing of Offshore Structures," no. October.
[21] Wang, X., Amdahl, J., and Egeland, O., 2022, "Numerical study on buckling of aluminum extruded panels considering welding effects," Marine Structures, 84, p. 103230.
[22] Wang, X., and Amdahl, J., "Analysis of Welding Influences on Extruded Aluminum Panel Buckling," Proc. ASME 2022 41st International Conference on Ocean, Offshore and Arctic EngineeringV002T02A073.
[23] Veritas, D. N., 2015, "DNVGL-CG-0128 Buckling," Class guideline-Buckling, Edition October.
[24] Veritas, D. N., 2021, "DNV-CG-0128 Buckling," Class guideline-Buckling, Edition October.
[25] Standard, B., 2007, "Eurocode 9—Design of aluminium structures—."
[26] GL, D., 2019, "Rules for classification: high speed and light craft (RU-HSLC)," DNV GL AS Norway.
[27] Solland, G., and Jensen, P. l. G., 2004, "Background to DNV Recommended Practice DNV-RP-C201 Buckling Strength of Plated Structures," pp. 979-986.